JCTC Journal of Chemical Theory and Computation

Article

pubs.acs.org/JCTC

Effects from Spin−Orbit Coupling on Electron−Nucleus Hyperfine Coupling Calculated at the Restricted Active Space Level for Kramers Doublets

Kamal Sharkas, Ben Pritchard, and Jochen Autschbach*

Department of Chemistry, State University of New York at Buffalo, Buffalo, New York 14260-3000, United States

ABSTRACT: Calculations of electron−nucleus hyperfine coupling were implemented at the restricted active space state interaction (RASSI) level to treat spin−orbit (SO) coupling, based on scalar relativistic restricted active space wave functions. The current implementation is suitable for light atomic systems, for light ligand atoms in heavy metal complexes, and for spin−orbit coupling-induced hyperfine coupling of heavy atoms if the unpaired electrons are described by orbitals with high angular momentum. Spin polarization is reasonably well treated by allowing one hole and one electron in a window of active orbitals ('ras1', 'ras3') surrounding the principal active space ('ras2'). A benchmark set of Kramers doublet states of molecules with light and heavy atoms is used to evaluate the approach and verify the implementation. For NpF_6, the impact of SO coupling on the Np and F hyperfine coupling tensors is investigated in detail. It is demonstrated that the Np hyperfine coupling is strongly dominated by SO effects, that there is a large SO effect on the F hyperfine tensor components, and that SO coupling causes the fluorine dipolar term to acquire an isotropic component.

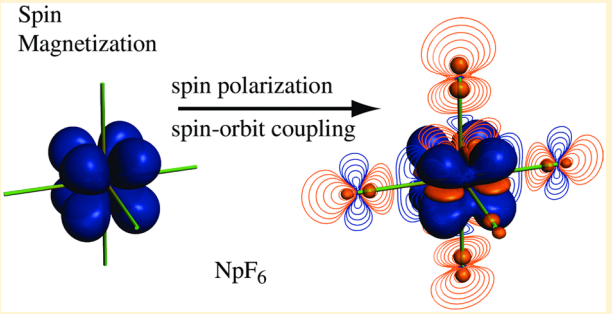

1. INTRODUCTION

Electron paramagnetic resonance (EPR) spectra can be modeled by a spin Hamiltonian affording a few key parameters: the Zeeman coupling matrix ("*g*-tensor") and the *g*-factors, the zero-field splitting parameters, and the electron−nucleus hyperfine coupling (HFC) matrix ("hyperfine tensor") and the associated HFC constants (HFCCs).[1−3] The numerical values of these quantities are commonly obtained by fitting the eigenvalues of the effective spin (pseudospin) Hamiltonian to the measured spectrum. Reliable computational predictions for the spin Hamiltonian parameters from quantum chemical methods are important for gaining insight about structure and bonding from measured spectra.[4,5] This work is concerned with hyperfine coupling, which describes the interaction between the electron spin and nuclear spins in paramagnetic molecules. It is important to describe properly the electron correlation and relativistic effects on HFC, because it is sensitive to both.

Much research has been invested in the treatment of the nonrelativistic limit where HFC is dominated by the Fermi contact (FC) and the spin-dipole (SD) mechanisms. In this case, ab initio theories that have been evaluated range from approximations neglecting electron correlation to high-level approaches that tackle the electron correlation in different ways. There is, in particular, the difficulty of treating spin polarization, as HFC is very sensitive to the balance of the α-spin versus β-spin density distribution at and around a nucleus of interest. At the noncorrelated Hartree−Fock (HF) level and its semi-empirical variants,[6,7] spin polarization is explicitly included in spin-unrestricted calculations,[8−10] but often with the caveat of symmetry breaking or severe spin contamination. Correlated methods such as many-body perturbation theory,[11−16] coupled cluster,[11,17] and configuration interaction (CI)[10,18−23] theory have also been tested in HFC calculations. Kohn−Sham density-functional theory (KS-DFT)[24,25] is in widespread use because electron correlation effects are efficiently included via approximate exchange-correlation functionals. Various classes of functionals have been tested for their suitability in HFC calculations, such as the local spin density (LSD) approximation,[26] the generalized gradient approximation (GGA),[27−30] meta-GGAs,[31] global hybrids,[30] double hybrids,[31] and hybrids with range-separated exchange.[32,33]

In many situations, such as for (nearly or actual) orbitally degenerate electronic states, methods with single-determinant references may not yield a satisfactory description of the electronic structures of the investigated systems. A remedy is to use multiconfigurational methods such as multireference configuration interaction.[34−43] If the chosen method affords small active spaces, spin polarization may not be obtained adequately. In the restricted-unrestricted approach,[44] a spin-restricted multiconfigurational wave function responds to the hyperfine perturbation in an unrestricted manner describing the spin polarization of core orbitals. Another possibility is combining the density matrix renormalization group (DMRG) algorithm with the complete active space self-consistent field (CASSCF) method.[45,46] An advantage of this

Received: November 4, 2014
Published: December 19, 2014

DOI: 10.1021/ct500988h
J. Chem. Theory Comput. 2015, 11, 538−549

approach is that DMRG allows for a larger complete active space (CAS) than those constructed in traditional CASSCF, which facilitates the treatment of correlation as well as spin polarization. Although KS-DFT utilizes a single-determinant reference for the noninteracting system, it sometimes leads to reasonable HFCCs for systems with multireference character. This has been attributed to fortuitous error cancellations via the self-interaction error in present day functionals or via spin contamination in spin-unrestricted DFT.[47,48]

The importance of relativistic effects on HFC and other molecular properties related to the hyperfine Hamiltonian was already emphasized by Pyykkö in early reviews about relativistic quantum chemistry, for example in ref 49. Contributions from orbitals with large *s* character are of decisive importance for the FC term, which often dominates the HFC. Here, scalar relativistic effects[50] may contribute very significantly to HFCCs and even finite-nucleus effects may reach double digit percentage points. Scalar relativistic (SR) variants of approximate two-component operators, such as those based on the Douglas−Kroll−Hess (DKH) transformation,[46,51−53] and regular approximations to zeroth order (ZORA)[54,55] or infinite order,[56] provide efficient variational schemes by which to include scalar relativistic effects in HFC calculations. Scalar variants of fully decoupled two-component operators, for instance, via normalized elimination of the small component, have also been used in conjunction with wave function theory (WFT)[57] and DFT.[58] For situations where spin−orbit (SO) coupling is significant, SR and SO effects can both be included variationally, either at a two-component[54,55,59,60] or within a four-component relativistic framework.[61,62] Another possibility is to include SO effects on EPR parameters as a linear perturbation,[30,54,55,60,63] although the approach has its limitations.[64] In the framework of multireference wave function theory, SOC can be treated self-consistently, as reported for EPR *g*-factors in ref 65−67, or a posteriori[68,69] using the spin−orbit restricted active space state interaction (SO-RASSI)[70,71] approach as implemented, for instance, in the Molcas package.[72] In the SO-RASSI approach, a set of CAS or restricted active space (RAS) wave functions from a scalar relativistic multireference calculation form a basis in which the SO Hamiltonian is represented and diagonalized.

For the present study, we have implemented a new route toward calculating HFC within a RAS framework, which follows conceptually the approach for EPR *g*-factors of Bolvin.[68] For this purpose, a new module has been added to the RASSI program of the Molcas package. Based on scalar relativistic wave functions obtained with a variationally stable all-electron relativistic Hamiltonian, HFC and SO effects thereupon are introduced subsequently in the SO state-interaction step. At present, the implementation is suitable for light atomic systems, for light ligand atoms in heavy metal complexes (a major interest in our group's research), and for SO coupling-induced HFC of heavy atoms if the unpaired electrons are described by orbitals with high angular momentum, due to the use of nonrelativistic hyperfine operators. In subsequent work, the set of operators will be extended for general applications. We assess the performance via results obtained for a well-characterized benchmark set of molecules with Kramers doublet ground states in comparison with data from various HF and DFT schemes developed previously in our group for relativistic HFC calculations[33,54,55,73] and with experimental data, where available. A particular focus is on spin polarization transferred to ligand atoms and on SO effects induced by a heavy metal center on HFC of a light ligand atom.

The article is organized as follows: In Section 2, we review theoretical details and outline the implementation. Computational details are provided in Section 3. Results obtained with various methods for a test set of molecules with light to heavy atoms are presented and discussed in Section 4. Section 5 summarizes our findings.

2. METHODOLOGY

Hartree atomic units with $e = 1$, $m_e = \hbar = 1$, $4\pi\varepsilon_0 = 1$, $c = \alpha^{-1} \approx 137.036$, $\mu_0/(4\pi) = c^{-2}$ are used unless explicitly noted otherwise. The clamped-nucleus approximation is adopted. The symbols $\cdot$ and $\times$ indicate inner and outer products, respectively for vectors and tensors. Bold-italic notation such as $\boldsymbol{r}$, $\boldsymbol{S}$ is used for vectors and vector operators, while upright-bold such as $\mathbf{a}$, $\mathbf{g}$ is used for matrices and rank-2 tensors.

2.1. Hyperfine Coupling Perturbation Operators. The formalism closely follows the one implemented in the RASSI program of the Molcas package[72] for calculations of EPR *g*-factors. We shall therefore only briefly outline the approach. As it is the case for the EPR *g*-factor module in the SO-RASSI program, the HFC perturbation operators are currently nonrelativistic. This allows applications to light atomic systems, HFC of light ligand atoms in heavy metal complexes, and to study hyperfine coupling of heavy atoms induced by SO coupling if the unpaired orbitals have high angular momentum. Additional comments are provided in Section 2.2. The nonrelativistic one-electron Hamiltonian with spin in the absence of external magnetic fields or magnetic fields arising from nuclear spins reads

$$h_0 = V_{\mathrm{Ne}} + \frac{1}{2}(\boldsymbol{\sigma}\cdot\boldsymbol{p})(\boldsymbol{\sigma}\cdot\boldsymbol{p}) \tag{1}$$

where V_{Ne} is the interaction of the electron with the potential from the atomic nuclei, $\boldsymbol{\sigma}$ is the 3-vector of the 2×2 Pauli spin matrices, and $\boldsymbol{p} = -i\nabla$ is the linear momentum operator. As written, $(\boldsymbol{\sigma}\cdot\boldsymbol{p})(\boldsymbol{\sigma}\cdot\boldsymbol{p})$ is equal to $\boldsymbol{p}\cdot\boldsymbol{p}$ times a 2 by 2 unit matrix. One can then select an arbitrary spin quantization axis (usually z) and set up a spin-unrestricted or spin-restricted scheme with the usual scalar operator $h_0 = V_{\mathrm{Ne}} + 1/2\boldsymbol{p}\cdot\boldsymbol{p}$. However, in order to include SO effects on HFC the starting point is eq 1.

The hyperfine magnetic field for nucleus N is introduced by minimal substitution, $\boldsymbol{p} \rightarrow \boldsymbol{p} + \boldsymbol{A}_{\mathrm{N}}$, with $\boldsymbol{A}_{\mathrm{N}}$ being the magnetic vector potential associated with a nuclear spin, which gives

$$\begin{aligned} h &= V_{\mathrm{Ne}} + \frac{1}{2}(\boldsymbol{p}^2 + \boldsymbol{p}\cdot\boldsymbol{A}_{\mathrm{N}} + \boldsymbol{A}_{\mathrm{N}}\cdot\boldsymbol{p} + i\boldsymbol{\sigma}\cdot\{\boldsymbol{p}\times\boldsymbol{A}_{\mathrm{N}}\} \\ &\quad + \boldsymbol{A}_{\mathrm{N}}\cdot\boldsymbol{A}_{\mathrm{N}}) \\ &= h_0 + h_{\mathrm{N}} \end{aligned} \tag{2}$$

Here, h_{N} describes the magnetic hyperfine interactions between an electron and nucleus N. Curly brackets, $\{\cdots\}$, in the operator expressions indicate that derivatives are only taken inside the operator, not of functions on its right-hand side. The vector potential for a selected nucleus N in the point-dipole approximation is given in Coulomb gauge ($\nabla\cdot\boldsymbol{A}_{\mathrm{N}} = 0$) by

$$\boldsymbol{A}_{\mathrm{N}} = \frac{1}{c^2}\frac{\boldsymbol{m}_{\mathrm{N}}\times\boldsymbol{r}_{\mathrm{N}}}{r_{\mathrm{N}}^3} \tag{3}$$

Here, $\boldsymbol{r}_{\mathrm{N}}$ is the electron−nucleus distance vector and r_{N} its length. The nuclear magnetic moment $\boldsymbol{m}_{\mathrm{N}} = g_{\mathrm{N}}\beta_{\mathrm{N}}\boldsymbol{I}_{\mathrm{N}}$ is

DOI: 10.1021/ct500988h
J. Chem. Theory Comput. 2015, 11, 538−549

associated with the nuclear spin $\boldsymbol{I}_N$ via the nuclear g-factor (g_N) and the nuclear magneton (β_N). The factor of c^{-2} results from a conversion of $\mu_0/4\pi$ from SI to atomic units. Substitution of eq 3 in 2 gives

$$h_N = \frac{1}{c^2}\boldsymbol{m}_N\cdot\left(\frac{\boldsymbol{r}_N}{r_N^3}\times\boldsymbol{p}\right) + \frac{1}{2c^2}\boldsymbol{\sigma}\cdot\left\{\boldsymbol{m}_N\left(\nabla\cdot\frac{\boldsymbol{r}_N}{r_N^3}\right) - (\boldsymbol{m}_N\cdot\nabla)\frac{\boldsymbol{r}_N}{r_N^3}\right\} + \frac{1}{2}\boldsymbol{A}_N\cdot\boldsymbol{A}_N \tag{4}$$

For calculations of hyperfine perturbations, the derivative

$$h_{N,u} = \left.\frac{\partial h_N}{\partial I_{N,u}}\right|_{\boldsymbol{I}_N=0} = h_{N,u}^{PSO} + (h_{N,u}^{FC} + h_{N,u}^{SD}) = \frac{g_N\beta_N}{c^2}\left(\frac{\boldsymbol{r}_N}{r_N^3}\times\boldsymbol{p}\right)_u + \frac{g_N\beta_N}{2c^2}\left\{\sigma_u\nabla\cdot\frac{\boldsymbol{r}_N}{r_N^3} - \boldsymbol{\sigma}\cdot\nabla_u\frac{\boldsymbol{r}_N}{r_N^3}\right\} \tag{5}$$

is needed. Subscript u indicates the x, y, or z component of a vector. The term that is bilinear in $\boldsymbol{A}_N$ in eq 4 does not contribute to $h_{N,u}$ since the derivative is taken at $\boldsymbol{I}_N = 0$. A bilinear derivative of $1/2\sum_{M,N}\boldsymbol{A}_N\cdot\boldsymbol{A}_M$ is responsible for the diamagnetic spin−orbital (DSO) mechanism of indirect nuclear spin−spin coupling (J-coupling) when eq 3 represents the vector potential of two or more nuclei instead of a single nucleus.

The electron-spin independent part of 5 is the time-odd paramagnetic spin−orbital (PSO) perturbation operator (sometimes labeled OP for "orbital paramagnetic"). The electron-spin dependent hyperfine terms (containing $\boldsymbol{\sigma}$) in eq 5 represent the sum of the time-odd Fermi-contact (FC) and spin-dipole (SD) operators. These operators contribute to the NMR shielding and J-coupling of closed-shell molecules at the nonrelativistic limit because NMR shielding and J-coupling are double perturbation properties where the second perturbation—from the external magnetic field or the hyperfine field of another nucleus—is also time-odd. In contrast, HFC is calculated from the unperturbed wave function akin to a first-order property, in which case the hyperfine operators only have non-zero matrix elements if the electronic state of interest is degenerate. In the absence of orbital degeneracies or strong SO coupling, the PSO contribution to HFC vanishes. In this work, we study two cases (NpF_6, UF_6^-) where large PSO contributions to HFC arise from SO coupling.

The FC operator itself is given by 2/3 of the term $(g_N\beta_N)/(2c^2)\sigma_u\nabla\cdot(\boldsymbol{r}_N/r_N^3)$ of eq 5.[74] Its usual representation with a Dirac delta distribution is obtained by using the identity $\nabla\cdot\boldsymbol{r}_N/r_N^3 = 4\pi\delta(\boldsymbol{r}_N)$, which gives the well-known expression

$$h_{N,u}^{FC} = \frac{4\pi}{3c^2}\sigma_u\delta(\mathbf{r}_N) \tag{6}$$

In the absence of SO coupling, the SD operator gives rise to an anisotropic HFC matrix; that is, it does not contribute to the isotropic HFCC but it is essential when the tensor properties of HFC are of interest. The SD operator samples the spin magnetization distribution around the nucleus of interest. An isotropic SD component may be generated in the presence of SO coupling as we shall demonstrate below. Relativistic versions of the "contact" term, and its variants derived for finite nuclear models, also sample the spin density over a finite volume rather than just at the location of a (point) nucleus.

The calculation of FC and SD matrix elements in a basis of a selected set of CAS or RAS wave functions and, subsequently, in the basis of SO-RASSI wave functions, was enabled in a new module "ATENS" in the Molcas package as follows: For a given Cartesian component u, the electron-spin dependent operators in eq 5 can be written as $f_u(\boldsymbol{r})\sigma_u$, with f_u being some operator depending on the electron coordinate $\boldsymbol{r}$ but not on the electron spin. For FC and SD, nonrelativistically, apart from pre-factors, the spatial operators f_u happen to be the same as those for the electric-field gradient (EFG), for which integrals over the atomic orbital (AO) basis were already available. The construction of the SO Hamiltonian in the RASSI code is also based on processing AO matrix elements indexed by some Cartesian component u, times the electron spin operator for direction u. Therefore, the task was essentially accomplished by processing EFG AO integrals in a module closely resembling the one that constructs the SO operator matrix representation in RASSI. Further details can be found in the PhD thesis of one of the authors (B.P.).[75] PSO integrals in the AO basis were not previously available. These have been newly added to the "seward" module of Molcas via interfacing the integral-derivative library GEN1INT by Gao et al.[76]

2.2. Hyperfine Coupling Implementation within the SO-RASSI Framework. We adapt the strategy for calculations of electronic g-factors within the SO-RASSI framework[68,69] for the purpose of HFC calculations. The EPR spin Hamiltonian describing the HFC of nucleus N,

$$H_N^{HFC} = \boldsymbol{I}_N\cdot\mathbf{a}_N\cdot\boldsymbol{S} \tag{7}$$

couples the nuclear spin vector $\boldsymbol{I}_N$ with the pseudospin operator $\boldsymbol{S}$ of the electronic system. The 3×3 matrix $\mathbf{a}_N$ describes the hyperfine coupling. For calculations of EPR g-factors, the spin Hamiltonian is the Zeeman interaction $H_N^Z = \boldsymbol{B}\cdot\mathbf{g}\cdot\boldsymbol{S}$, with $\boldsymbol{B}$ being the external magnetic field. Therefore, a code for calculating the elements of the Zeeman coupling matrix $\mathbf{g}$ can be adapted to calculate the HFC matrix $\mathbf{a}_N$ by replacing matrix elements of the Zeeman operator h_u^Z with matrix elements of the HFC perturbation operator of eq 5. In the "nonrelativistic with spin" limit, $h_u^Z = \partial h(\boldsymbol{B})/\partial B_u|_{B=0} = (L_u + \sigma_u)/2$, with L_u being a component of the one-electron orbital angular momentum vector operator.

Following ref 68, the components of the rank-2 tensor $\mathbf{a}_N\mathbf{a}_N^T$ are given in the basis of the SO-RASSI Kramers doublet components $|i\rangle$, $|j\rangle$ by the following expression:[77]

$$(\mathbf{a}_N\mathbf{a}_N^T)_{uv} = 2\sum_{i,j}\langle i|h_{N,u}^{PSO} + h_{N,u}^{FC} + h_{N,u}^{SD}|j\rangle\langle j|h_{N,v}^{PSO} + h_{N,v}^{FC} + h_{N,v}^{SD}|i\rangle \tag{8}$$

($u,v \in \{x, y, z\}$). The principal HFC components are then extracted from diagonalizing this tensor as described in Section 3. The principal axis system is given by the eigenvectors. Expression 8 is analogous to the equation used to calculate g-factors within the SO-RASSI framework.[68,69,77] The imaginary PSO operator replaces L_u, L_v of the g-tensor expression, and the electron-spin dependent (FC+SD) parts of the HFC operator replace σ_u, σ_v. The wave functions of the Kramers doublet are first obtained in a spin-free CAS or RAS representation, based on the DKH2 operator to include the scalar relativistic effects. Then the SO coupling is accounted for in the SO-RASSI step,

DOI: 10.1021/ct500988h
J. Chem. Theory Comput. 2015, 11, 538−549

with a SO Hamiltonian calculated from the atomic mean-field integral approximation (AMFI).[78−80]

Limitations of using the operator in eq 5 for HFC calculations arise from the fact that electron density and spin density due to s and $p_{1/2}$ orbitals of heavy atoms increases very strongly in the vicinity of the nucleus due to direct relativistic effects[50,81] (with a point nucleus there is a logarithmic divergence relativistically, which, however, is not represented by the Gaussian-type basis sets used in most calculations). A matching relativistic "contact" operator that does not sample the spin density right at the nuclear position must then be used. For light neighboring atoms, the relativistic effects originate in the valence shell of the heavy atom, while the magnetic perturbation operators for the light neighbor nucleus are well approximated by nonrelativistic operators due to their locality. A similar argument can be made about outer core and valence shells of the heavy atom with high angular momentum, as they have vanishingly small electron and spin density near the heavy nucleus and the relativistic effects are indirect[50,81] rather than direct. The approximations introduce a form of "picture change" error, which would be very severe for orbitals of heavy atoms with low angular momentum. We intend to implement a scheme with matching relativistic operators for the external-field free and the hyperfine Hamiltonian in the near future. One of the major areas of intended applications, namely the study of HFC of ligand atoms in heavy metal complexes (and paramagnetic chemical shifts,[32] which depend on the HFC) can already be pursued with the current implementation, as we demonstrate herein.

3. COMPUTATIONAL DETAILS

Calculations have been performed with a locally modified version of the 2014 developer's version of Molcas[72] using the restricted active space (RAS) model. Scalar relativistic effects were included in the wave function calculations using the DKH2 Hamiltonian.[82,83] Based on eq 8, HFC tensors were obtained with the SO-RASSI module as described in Section 2.2, with nonrelativistic operators as discussed above.

For comparison, HFC tensors were also calculated using a locally modified version of the open source NWChem package[84] where three methods for HFC based on the ZORA relativistic Hamiltonian were recently implemented and evaluated with DFT and HF theory by our group.[54,55] These methods are (i) calculations where SO coupling is treated as a perturbation to obtain the effects from the PSO operator via linear response (referred to as the LR scheme), based on a spin-polarized spin-unrestricted scalar relativistic reference; (ii) a Kramers-doublet method devised originally by van Lenthe, Wormer, and van der Avoird (LWA)[59] where SO coupling is treated variationally, but within a non-spin-polarized two-component relativistic framework; (iii) variational calculations including SO coupling with a generalized-collinear spin-polarized two-component relativistic reference, using different orientations of the spin-quantization axis. The latter approach was inspired by a method[85] for calculating magnetic anisotropy (MA) with DFT and is therefore referred to as the MA route to HFC. We note that—unless the influence of SO coupling on the HFC tensor is significant or certain symmetry considerations apply—the LR and MA approaches yield equivalent results. Comparisons with LWA data are used in the present work to investigate the effects from lack of spin polarization, which are usually severe for HFC. The LR, LWA, and MA calculations of HFCCs were carried out at the Hartree−Fock (HF) level and with DFT using the global hybrid Perdew−Burke−Ernzerhof functional with 25% exact exchange (PBE0).[86]

The molecule test set is comprised of two subsets of molecules with Kramers doublet ground states. Subset I contains radicals with light and moderately heavy elements: CH_3, HCO, HSiO, HSiS, SiOH, SiSH, and TiF_3. Subset II contains radicals with heavy elements: HgH, HgF, NpF_6, and UF_6^-. Optimized geometries for CH_3, HCO, HSiO, HSiS, SiOH, SiSH, TiF_3, HgH, HgF were taken from ref 73 (optimized with the Amsterdam Density Functional (ADF) code[87] with scalar ZORA, the Becke−Perdew (BP) functional,[88,89] and a triple-ζ doubly polarized (TZ2P) Slater-type basis). CASPT2 geometries for NpF_6 and UF_6^- were taken from ref 90. The following nuclear g-factors[91−93] were employed to convert the calculated HFCs from atomic units to MHz: $g_{1_H} = 5.5857$, $g_{13_C} = 1.4048$, $g_{17_O} = -0.7575$, $g_{19_F} = 5.25773$, $g_{29_{Si}} = -1.11057$, $g_{33_S} = 0.42921$, $g_{47_{Ti}} = -0.31539$, $g_{235_U} = -0.1228$, $g_{237_{Np}} = 1.2560$. All-electron basis sets ANO-RCC contracted to triple-ζ quality[94−96] were used with uncontracted s functions on H ($8s4p3d1f/8s2p1d$), C, O, F ($14s9p4d3f2g/14s3p2d1f$), S, Si ($17s12p5d4f2g/17s4p2d1f$), and Ti ($21s15p10d6f4g2h/21s5p3d2f1g$). The basis sets were fully uncontracted for Np and U for the NWChem calculations because they became extremely slow with high contractions. For the Molcas calculations, the U and Np basis sets were contracted as $26s23p17d13f5g3h/9s8p6d4f2g1h$. The point-nucleus approximation was used throughout. Finite-nucleus effects can be large for heavy nuclei if the HFC is dominated by the FC mechanism,[54,55] but as discussed in Section 2.2, such cases are not within the scope of the present study.

The SO-RASSI calculations started out with a HF self-consistent field (SCF) calculation for a corresponding closed-shell system with one less electron. Then, a calculation was carried out with a "ras2" minimal active space comprising, for the majority of considered molecules, simply the unpaired electron in the first N low-lying virtual HF orbitals, that is, CAS(1,N) which is, for our samples, not unlike restricted open-shell HF. There is no unique strategy to determine N. A minimal active space calculation is expected to suffer from lack of spin polarization, similar to the LWA approach. After some preliminary test calculations, for each system, we chose a ras2 space yielding HFCCs close to those obtained with LWA/HF, especially for the systems with light atoms. For molecules containing moderately heavy or heavy elements, the minimal CAS has been chosen to include the orbitals which are known to be important in the considered molecule. For TiF_3, the minimal CAS(1,5) comprises one electron in five $3d/4s$ hybrid orbitals. CAS(3,7) is augmented by titanium $1s$ and another $4s$-rich orbital. For HgH and HgF, CAS(3,6) consists of three electrons in six orbitals with large $6s$ and $6p$ character. For NpF_6 and UF_6^-, in CAS(1,7), the active space is comprised of the seven $5f$ orbitals on the actinide center. The optimized orbitals from these CAS calculations were then used as starting points for subsequent calculations with the same orbitals assigned to ras2, but in which additional spin polarization was introduced in the wave functions—without further orbital optimization—by allowing for one hole to be created in the "ras1" space and one electron to be created in the "ras3" space. The ras1/ras3 active spaces have been chosen to include as many unoccupied orbitals as possible and to obtain reasonably well converged results with respect to the number of included

DOI: 10.1021/ct500988h
J. Chem. Theory Comput. 2015, 11, 538−549

Table 1. Isotropic Hyperfine Coupling Constants (MHz) for Molecule Set I Calculated with Different Approaches Described in Section 3[a]

		SO-RASSI				HF			PBE0			
	active space	FC+SD	PSO	total		FC+SD	PSO	total	FC+SD	PSO	total	exp.
CH_3												
C	CAS(1,8)	2.13	0.01	2.11	LR	169	−0.17	168	85.2	−0.14	85.0	108[b]
C	RAS[4/5]	99.7	0.03	99.7	MA			168			85.0	
C	RAS[4/20]	131	0.02	131	LWA			−0.02			−0.02	
C	RAS[4/60]	130	0.02	130								
H	CAS(1,8)	0.00	0.00	0.00	LR	−119	0.01	−119	−70.1	0.02	−70.1	−64.5[b]
H	RAS[4/5]	12.1	0.00	12.1	MA			−119			−70.1	
H	RAS[4/20]	46.3	0.00	46.3	LWA			−0.02			−0.02	
H	RAS[4/60]	62.0	0.00	62.0								
HCO												
C	CAS(1,8)	299	0.22	299	LR	444	−0.50	444	384	−0.50	384	365[c]
C	RAS[7/15]	386	0.32	387	MA			444			384	
C	RAS[7/30]	395	0.39	396	LWA			270			330	
C	RAS[7/70]	395	0.40	396								
H	CAS(1,8)	333	0.05	333	LR	376	−0.08	376	361	−0.08	361	354[c]
H	RAS[7/15]	353	0.08	353	MA			376			360	
H	RAS[7/30]	348	0.09	349	LWA			307			315	
H	RAS[7/70]	363	0.09	363								
O	CAS(1,8)	10.8	0.21	11.0	LR	−62.4	0.30	−62.1	−33.6	0.38	−33.3	
O	RAS[7/15]	61.8	0.17	61.9	MA			−62.0			−33.2	
O	RAS[7/30]	73.0	0.23	73.0	LWA			−31.0			−14.0	
O	RAS[7/70]	60.0	0.26	60.2								
HSiO												
Si	CAS(1,15)	638	0.27	638	LR	−602	0.23	−602	−548	0.26	−548	−630[d]
Si	RAS[7/30]	646	0.52	646	MA			−602			−548	
Si	RAS[7/50]	641	0.53	642	LWA			−519			−563	
Si	RAS[7/75]	641	0.53	641								
H	CAS(1,15)	279	0.03	279	LR	437	−0.03	437	417	−0.03	417	450[d]
H	RAS[7/30]	364	0.03	365	MA			437			417	
H	RAS[7/50]	375	0.03	375	LWA			265			321	
H	RAS[7/75]	375	0.03	375								
O	CAS(1,15)	4.03	0.13	4.16	LR	−41.6	−0.17	−41.8	−11.3	0.00	−11.3	
O	RAS[7/30]	55.6	0.34	55.4	MA			−41.7			−11.3	
O	RAS[7/50]	72.6	0.37	72.4	LWA			−18.0			−5.32	
O	RAS[7/75]	72.8	0.37	72.6								
HSiS												
Si	CAS(1,8)	520	0.60	521	LR	−570	0.94	−569	−509	0.98	−508	
Si	RAS[5/10]	569	0.76	569	MA			−569			−508	
Si	RAS[5/80]	540	1.20	541	LWA			−399			−489	
Si	RAS[10/75]	606	1.30	607								
Si	RAS[15/85]	610	1.31	611								
H	CAS(1,8)	197	0.06	197	LR	326	−0.07	326	316	−0.07	316	
H	RAS[5/10]	207	0.08	208	MA			326			316	
H	RAS[5/80]	272	0.08	272	LWA			181			235	
H	RAS[10/75]	272	0.08	272								
H	RAS[15/85]	272	0.08	272								
S	CAS(1,8)	3.12	0.27	3.73	LR	6.35	0.86	7.21	1.29	0.78	2.07	
S	RAS[5/10]	6.02	0.68	5.33	MA			7.11			2.00	
S	RAS[5/80]	23.1	0.68	22.5	LWA			5.36			5.96	
S	RAS[10/75]	23.1	0.68	22.4								
S	RAS[15/85]	18.1	0.53	20.6								
SiOH												
O	CAS(1,8)	10.8	0.57	11.4	LR	−26.9	0.44	−26.5	−21.3	0.65	−20.6	
O	RAS[5/35]	11.4	0.69	12.0	MA			−26.5			−20.6	
O	RAS[5/75]	15.2	0.82	16.0	LWA			−9.46			−15.8	
O	RAS[7/65]	15.4	0.85	16.1								
O	RAS[11/85]	10.4	0.87	11.1								

DOI: 10.1021/ct500988h
J. Chem. Theory Comput. 2015, 11, 538−549

Table 1. continued

		SO-RASSI				HF			PBE0			
	active space	FC+SD	PSO	total		FC+SD	PSO	total	FC+SD	PSO	total	exp.
SiOH												
Si	CAS(1,8)	1.03	5.66	6.74	LR	−42.9	3.72	−39.2	19.7	4.89	24.6	
Si	RAS[5/35]	89.6	5.71	95.2	MA			−39.0			24.7	
Si	RAS[5/75]	64.7	5.77	71.0	LWA			−14.0			38.5	
Si	RAS[7/65]	66.0	5.84	72.6								
Si	RAS[11/85]	65.1	6.42	71.6								
H	CAS(1,8)	35.3	0.18	35.4	LR	42.7	−0.09	42.6	50.1	−0.13	50.0	
H	RAS[5/35]	38.0	0.18	38.1	MA			42.3			50.0	
H	RAS[5/75]	39.3	0.18	39.4	LWA			33.5			43.6	
H	RAS[7/65]	39.2	0.19	39.4								
H	RAS[11/85]	39.3	0.19	39.5								
SiSH												
S	CAS(1,8)	21.7	0.15	21.8	LR	12.3	−0.18	12.1	20.3	−0.21	20.1	
S	RAS[5/35]	8.12	0.14	8.17	MA			12.1			20.1	
S	RAS[5/80]	8.36	0.14	8.42	LWA			16.2			27.7	
S	RAS[7/65]	8.36	0.15	8.42								
S	RAS[12/85]	8.40	0.16	8.47								
Si	CAS(1,8)	0.07	3.15	3.22	LR	−62.3	2.69	−59.7	15.9	3.07	18.9	
Si	RAS[5/35]	85.0	2.71	82.2	MA			−59.4			19.1	
Si	RAS[5/80]	56.9	2.70	59.2	LWA			4.03			5.21	
Si	RAS[7/65]	58.2	2.85	61.3								
Si	RAS[12/85]	84.1	3.08	80.8								
H	CAS(1,8)	66.7	0.04	66.3	LR	105.2	−0.04	105	116	−0.06	115	
H	RAS[5/35]	84.6	0.04	84.6	MA			105			115	
H	RAS[5/80]	93.7	0.04	93.7	LWA			66.5			95.7	
H	RAS[7/65]	93.4	0.04	93.5								
H	RAS[12/85]	93.6	0.04	93.7								
TiF_3												
Ti	CAS(1,5)	272	8.36	280	LR	−127	5.27	−121	−199	3.20	−196	−185[e]
Ti	CAS(3,7)	234	6.64	241	MA			−121			−196	
Ti	RAS[3/8][f]	210	6.61	217	LWA			−222			−248	
F	CAS(1,5)	19.0	3.20	22.0	LR	−52.9	0.73	−52.2	−15.2	0.62	−14.6	−24[e]
F	CAS(3,7)	18.7	2.94	21.6	MA			−52.0			−16.8	
F	RAS[3/8][f]	31.0	2.94	29.0	LWA			−12.8			−16.1	

[a]RASSI data unsigned. Scalar spin-unrestricted ZORA $\langle S^2\rangle$ from HF/PBE0, with $\langle S^2\rangle_{exact}$ = 0.7500: CH_3 (0.7621/0.7548); HCO (0.7668/0.7544); HSiO (0.7791/0.7586); HSiS (0.7834/0.7594); SiOH (0.7776/0.7584); SiSH (0.7774/0.7590); TiF_3 (0.7536/0.7526). [b]Ref 98. [c]Ref 99. [d]Ref 100. [e]Ref 101. [f]Based on CAS(3,7).

occupied orbitals. To this end, a limit of 30 orbitals for the ras1 and ras3 spaces that was hard-coded in the RASSI program has been lifted to be able to obtain sufficient spin polarization. For HgH and HgF, ras1 is dominated by the set of 5*d* orbitals. For NpF_6 and UF_6^-, ras1 is essentially composed of the fluorine orbitals deriving from 2*p*, 2*s*, 1*s*. Another criterion for the selection of the active spaces was that all members or none of sets of related molecular orbitals (e.g., all metal−ligand σ and π bonding orbitals for the actinide complexes) should be included in a RAS subspace in order to avoid symmetry breaking of the wave function. Throughout this work, the size of the active space is denoted as RAS[*X*/*Y*], where *X* is the number of doubly occupied orbitals included in ras1 and *Y* is the number of unoccupied orbitals included in ras3, similar to the notation used in ref [67].

Use of the AMFI approximation for constructing the SO Hamiltonian avoids the calculation of multicenter spin−orbit integrals. Furthermore, a "partial AMFI" functionality introduced for a previous study[97] allows to disable contributions to the SO operator from selected types of atoms. We utilized this functionality to investigate the importance of SO effects on the HFC tensor of NpF_6.

In the LR calculations with NWChem,[54,55] the HFC matrix is calculated directly and the symmetric part is diagonalized. The signs of the HFC tensor components are reported as calculated. For the LWA, MA,[55] and SO-RASSI calculations, the principal HFC components a_N^i, i = 1,2,3, are obtained by diagonalizing the matrix $\mathbf{a}_N\mathbf{a}_N^T$ of eq 8 and taking the square root of the diagonal values, that is, $a_N^i = \pm\ ((\mathbf{a}_N\mathbf{a}_N^T)_{ii}^{diag})^{1/2}$, such that the sign information is lost. Signs of the components have been adjusted, where needed, to match the LR results and/or known experimental signs. The reported isotropic HFCCs are based on the signed tensor elements. For the LR and SO-RASSI calculations, separate contributions from PSO and FC + SD or FC and SD individually are also provided. In the SO-RASSI calculations, the individual terms were obtained by calculating the HFC tensor with only one set of operators, PSO, FC, or SD, respectively. These contributions are reported unsigned, but still based on the relative signs assigned to the principal total components to get isotropic averages. Due to the bilinear dependence of the $\mathbf{a}_N\mathbf{a}_N^T$ tensor on the different operators in eq

DOI: 10.1021/ct500988h
J. Chem. Theory Comput. 2015, 11, 538−549

Table 2. Isotropic Hyperfine Coupling Constants (MHz) for Molecule Set II Calculated with Different Approaches Described in Section 3[a]

		SO-RASSI				HF			PBE0			
	active space	FC+SD	PSO	total		FC+SD	PSO	total	FC+SD	PSO	total	exp.
HgH												
H	CAS(3,6)	611	0.98	611	LR	654	−1.28	653	677	−1.79	676	710[b]
H	RAS[1/50]	625	1.03	626	MA			655			672	
H	RAS[3/50]	665	0.97	666	LWA			268			438	
H	RAS[8/55]	691	0.97	691								
HgF												
F	CAS(3,6)	45.7	13.0	58.7	LR	505	−34.7	470	270	−100	170	578[c]
F	RAS[1/25]	22.9	54.8	77.7	MA			475			170	318[c]
F	RAS[5/75]	23.4	90.0	113	LWA			227			43.4	
NpF_6												
Np	CAS(1,7)	153	1626	1473	LR	1376	−3456	−2080	−208	−2187	−2395	−1995[d]
Np	RAS[5/20]	318	1623	1941	MA			−1587			−2229	
Np					LWA			−1540			−1740	
F	CAS(1,7)	9.00	18.0	27.0	LR	−184	−89.0	−273	−43.0	−21.0	−64.0	−73[d]
F	RAS[5/20]	39.0	7.00	46.0	MA			−221			−53.0	
F	RAS[5/65]	47.0	7.00	54.0	LWA			−44.0			−34.0	
F	RAS[13/65]	49.0	7.00	56.0								
F	RAS[16/65]	46.3	14.3	61.0								
UF_6^-												
U	CAS(1,7)[e]	17.0	146	129	LR	13.0	194	207	34.0	143	176	
U	RAS[5/20]	90.0	146	236	MA			167			166	
U					LWA			126			127	
F	CAS(1,7)	6.00	15.0	21.0	LR	−89.0	−24.0	−113	−40.0	−10.0	−50.0	
F	RAS[5/20]	21.0	6.00	27.0	MA			−94.0			−36.0	
F	RAS[16/65]	24.0	9.00	33.0	LWA			−17.0			−19.0	

[a]RASSI data unsigned. Scalar spin-unrestricted ZORA $\langle S^2\rangle$ from HF/PBE0, with $\langle S^2\rangle_{exact}$ = 0.7500: HgH (0.7906/0.7611); HgF (0.7675/0.7576); NpF_6 (0.8448/0.776); UF_6^- (0.7610/0.7580). [b]Ref 102. [c]1/3 of sum or difference of $a_{\|}$ and $2a_{\perp}$ from Table II in ref 103. [d]Ref 93. [e]The UF_6^- active spaces were selected based on the NpF_6 results.

8 the sum of individual terms may differ from the calculation with the full set of operators. The individual terms and the total HFCs are given with 3 to 4 significant figures, not with a set absolute precision, to facilitate comparisons between the different types of calculations.

4. RESULTS AND DISCUSSION

The present test set has been used by us previously[54,55,60] for assessing the performance of various relativistic DFT-based methods (and HF theory) developed for HFC calculations. It includes systems ranging from "nonrelativistic" molecules (Subset I) to structures with strong SOC (NpF_6 and UF_6^-). In these studies, and in related literature, spin polarization was shown to be very important for many of the HFCs of the test set. In spin-unrestricted HF and DFT calculations, spin polarization is easily obtained—but at the disadvantage of spin contamination and symmetry breaking. In CI-type calculations, the singles level of excitations, used in the present RAS calculations in conjunction with the principal "ras2" active space, is known to be the simplest spin polarization model that yields reasonably accurate predictions of HFCCs,[10] benefiting from some error cancellation by neglecting higher excitation levels.[23] Therefore, the discussion focuses on spin polarization effects and on the importance of SO coupling for the heavy-element systems. Subset I is mainly used to verify the implementation of the HFC expression and the correctness of the operator integrals and to assess the approach for obtaining spin polarization.

The comparison with the different HF and DFT methods provides additional information about spin polarization effects (LWA and CAS vs LR, MA, and RAS), SO effects, and the need for a treatment of SO coupling beyond first order (performance of LR versus MA and RAS at the spin-polarized level, and LWA vs CAS at the level without/with minimal spin polarization, and the overall magnitude of the PSO mechanism), and the importance of electron correlation.

4.1. Set I: Radicals with Light Main Group Atoms. Table 1 reports the isotropic hyperfine coupling constants (HFCC) for a test set of light molecules calculated by the various methods. All HFCCs are given in SI units of MHz. The FC + SD and PSO terms are provided separately. For these systems, SO coupling is small and the HFC is dominated by the contact and dipolar terms. However, we note that the orders of magnitude of the small PSO contributions are in-line with the HF and DFT LR calculations. In the latter, the PSO terms are available separately from the total results. A minor outlier is the fluorine HFC of TiF_3 where the PSO term is significantly larger with SO-RASSI than with the HF and PBE0 LR calculations, although it remains small compared to the total coupling, and more in line with ref 60.

The calculations show that spin polarization plays a decisive role in obtaining reliable estimates of the HFCCs for these systems. For most compounds in this set, the quasi-restricted LWA at the Hartree−Fock level and RASSI using the minimal active space tend to behave similarly. These calculations lack spin polarization, and consequently, they are not adequate to predict the HFCs accurately. The resulting HFCCs are

DOI: 10.1021/ct500988h
J. Chem. Theory Comput. 2015, 11, 538−549

generally lower in magnitude for the light atoms than the experimental values or spin-polarized HF and DFT. As an example, at the level of LWA and RAS with minimal active space, the spin density of CH_3 (originating from the carbon 2*p* orbital perpendicular to the molecule's plane) has effectively a node in the plane containing the carbon and hydrogen nuclei, and therefore, there is no FC contribution to the carbon HFC and the proton HFC vanishes. However, including carbon 2*s*, 1*s*, and the C−H bonding MOs in the active space, as in RAS[4/5], introduces a considerable amount of spin polarization and substantially improves the carbon HFC toward the spin-polarized (LR or MA) PBE0 results. With larger active spaces, PBE0 and RASSI bracket the experimental value by approximately equal amounts. The proton HFCs need a large ras1/3 active space to converge to reasonable values. At the RAS[4/60] level, the results are not far from experiment and PBE0. Similar trends can be observed for other members of Set I. The case of TiF_3 is also interesting. Here, with LWA or a small CAS RASSI calculation, the FC mechanism for Ti is quite strongly overestimated. The unpaired orbital is a titanium $3d_{z2}$/4*s* hybrid, and therefore, nonvanishing spin density at the Ti and F nuclei is already obtained without spin polarization. With a few orbitals added to the ras1/3 spaces, however, the results improve considerably for the Ti HFC, while not strongly deteriorating those for fluorine. We note some outliers, namely for S in HSiS and Si for SiOH and SiSH, where the larger RAS spaces lead to strongly overestimated FC terms. This could be an indication of nonrelativistic hyperfine operators not being appropriate for these cases.

Overall, when spin polarization is included via the ras1/3 single excitation mechanism in addition to the principal ("ras2") active space, we obtain reasonable agreement with available experimental data and with the NWChem reference values. The method is not designed to be highly accurate, but in comparison with experiment, it performs often better than spin-unrestricted HF for Set I. This is promising, as the SO-RASSI implementation is capable of treating systems where spin-unrestricted HF theory and KS-DFT would give severe symmetry breaking or spin contamination. Note that the small ras2 spaces used herein in conjunction with the one-hole one-electron ras1/ras3 setup are not expected to produce any significant electron correlation contributions to the molecular energy. Certainly, the calculated results for the hfc *and* the energy should improve further if dynamic correlation is treated more accurately in the wave functions.

4.2. Set II: Radicals with Transition Metals and Actinides. Results for molecule Set II are collected in Table 2. For the reasons given in Section 2, we focus on the ligand nuclei and on the Np HFC of NpF_6. We discuss the latter first.

When the active space is not extended to include core orbitals and outer core orbitals with low angular momentum, the neptunium HFC of NpF_6 remains numerically somewhat stable since it is strongly dominated by the PSO contribution from an orbital with high angular momentum. This assignment has already been verified in a previous study where the PSO term in a LR calculation was shown to originate almost exclusively from the unpaired Np 5*f* orbital.[54] With an active space that includes the Np 5*f* orbitals in ras2 and a small number of additional occupied frontier orbitals in ras1, there is excellent agreement with experiment, and we did not observe suspiciously large FC contributions. (Nonetheless, the FC + SD contributions for Np are to be considered with some caution. They will be revisited in subsequent work.) With the largest RAS spaces used to converge the fluorine HFC, the hyperfine coupling at the actinide center became contaminated with large spurious FC+SD contributions. These results, as well as those for U of UF_6^-, are consequently omitted from the table. At the CAS(1,7) SO-RASSI level, there is close agreement of the Np HFC with the LWA calculations, as one should expect. In the LR calculations for NpF_6, spin-unrestricted HF theory strongly overestimates the magnitude of the spin mechanism (FC+SD) of the Np HFC, and its positive sign appears to be unphysical. The negative PSO term is likewise strongly overestimated. Error cancellation brings the total LR/HF hyperfine coupling close to experiment. (For the fluorine nuclei, the two mechanisms afford the same sign and the LR/HF coupling is much too large in magnitude.) LR/PBE0 is better behaved but still overestimates the Np HFCC. At the MA level, HF and PBE0 bracket the experimental value, with HF too low in magnitude, and MA/PBE0 being too high but reasonably close. It was pointed out in ref 33 that the HFC shows a sensitive interdependence on how SO coupling is treated in spin polarized calculations versus the treatment of correlation and exchange.

The MA/PBE0 calculations perform quite well for F in NpF_6; the seemingly better performance of LR/PBE0 is most likely a case of error cancellation. In comparison, with a large RAS the SO-RASSI approach performs excellently and gives an isotropic fluorine HFCC that is also close to experiment. It needs to be pointed out that the measurements were performed on a solid, and therefore, one should not expect perfect agreement of gas phase calculations with measurements that may be affected to some degree by crystal packing. It is clear, however, that the RAS calculations with the largest active spaces deliver a reasonable amount of spin polarization. They also yield a sizable isotropic PSO component in the fluorine HFC without which the calculated SO result would be far from experiment. With CAS(1,7) the isotropic PSO contribution to the fluorine HFCC of NpF_6 is −18 MHz. The PSO term is reduced to −7 if spin polarization is introduced but the three bonding fluorine $2p_\sigma$ combinations are excluded from the active space. Once they are included in ras1 (RAS[16/*] versus RAS[5/*], RAS[13/*]), the isotropic PSO contribution rises again, to −14 MHz. This finding emphasizes the importance of ligand *p* orbitals in conjunction with strong SO coupling at the metal center in order to generate a sizable PSO mechanism. This is not surprising, since the corresponding operator has an angular momentum-like behavior around the nucleus of interest that is weighted by r_N^{-3}.

Since experimental results for UF_6^- are not available, we mainly provide the data here for benchmark purposes. An overall trend is that the fluorine HFC constants are smaller in magnitude than for NpF_6, which is found across the set of methodologies used. The RAS space that performs best for the fluorine nuclei of NpF_6 also gives for UF_6^- a fluorine HFCC that is close to the spin polarized DFT result obtained with MA/PBE0. At the metal center, the HFCs for U vs Np regarding the active space are roughly comparable if one divides the results by the nuclear *g*-factors (−0.1228 for ^{235}U and +1.256 for ^{237}Np).

In line with the importance of ligand *p* orbitals noted above, the H and F HFCCs for HgH and HgF, respectively, give a small PSO contribution for the former and a large one for the latter. Calculations with a minimal ras2 space (not shown) did not perform satisfactorily. After extending the ras2 active space by one more occupied orbital, the RAS results are in good agreement with experiment for HgH. The fluorine HFCC of

DOI: 10.1021/ct500988h
J. Chem. Theory Comput. 2015, 11, 538−549

Table 3. Hyperfine Coupling Matrix Components (MHz) for Np and F in NpF_6, with and without SO Effects, Calculated with SO-RASSI for Different Active Spaces[a]

		total			FC			SD			PSO		
	active space	$a_\perp$	$a_\parallel$	a_{iso}	$a_\perp$	$a_\parallel$	a_{iso}	$a_\perp$	$a_\parallel$	a_{iso}	$a_\perp$	$a_\parallel$	a_{iso}
	with SOC												
Np	CAS(1,7)	−1473	−1473	−1473	0.00	0.00	0.00	153	153	153	−1626	−1626	−1626
F	CAS(1,7)	−14.0	−53.0	−27.0	0.00	0.00	0.00	−6.00	−16.0	−9.00	−8.00	−37.0	−18.0
Np	RAS[5/20]	−1941	−1941	−1941	−479	−479	−479	161	161	161	−1623	−1623	−1623
F	RAS[5/20]	−24.0	−90.0	−46.0	−37.0	−37.0	−37.0	5.40	−16.0	−2.00	8.00	−37.0	−7.00
F	RAS[16/65]	−45.0	−92.0	−61.0	−45.0	−45.0	−45.0	−2.00	0.20	−1.27	2.00	−47.0	−14.3
	exp.[b]												
Np		−1995	−1995	−1995									
F		−42.0	−132	−73.0									
	previous calc.[c]												
Np		−2024	−2024	−2024									
F		−43.4	−103.2	−63.3									
	without SOC												
Np	CAS(1,7)	0.00	0.00	0.00	0.00	0.00	0.00	0.00	0.00	0.00	0.00	0.00	0.00
F	CAS(1,7)	9.00	−18.0	0.00	0.00	0.00	0.00	9.00	−18.0	0.00	0.00	0.00	0.00
Np	RAS[5/20]	−727	−727	−727	−727	−727	−727	0.00	0.00	0.00	0.00	0.00	0.00
F	RAS[5/20]	−41.0	−68.0	−50.0	−50.0	−50.0	−50.0	9.00	−18.0	0.00	0.00	0.00	0.00
F	RAS[16/65]	−73.0	−46.0	−64.0	−64.0	−64.0	−64.0	−9.00	18.0	0.00	0.00	0.00	0.00

[a]RASSI data signs assigned to match LR-PBE0. Additional HF and DFT calculations for NpF_6 were reported by us in refs 33, 54, and 105. [b]Experimental data from ref 93. [c]Dirac scattered wave calculations by Case, using nonrelativistic spin-unrestricted calculations to estimate spin polarization effects. Ref 104. ⊥, ||, and isotropic values for F. For Np, the three principal values are listed.

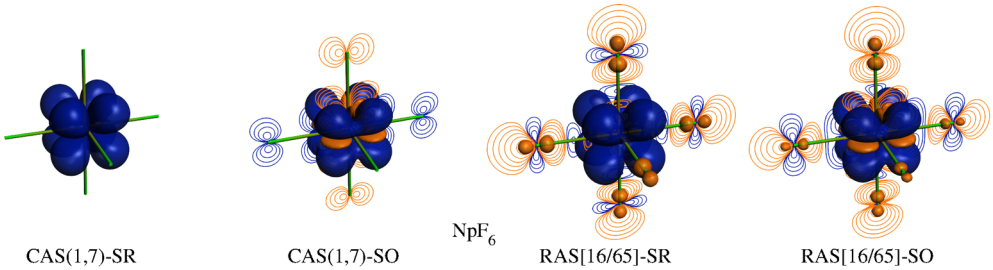

Figure 1. Spin magnetization m_z for NpF_6 for the ground state doublet component with $\langle S_z \rangle > 0$. For further details see text. Isosurface values: ± 0.003 atomic units. Contour lines in a plane containing four of the fluorine atoms with contour values from 10^{-4} to 1 with logarithmic spacing. For CAS(1,7)-SR, m_z shows no contributions in this plane. Blue/dark shading indicates positive m_z while orange/light shading indicates negative m_z. The z direction is vertical.

HgF is a very difficult case for DFT, as we noted already in a previous study.[55] There appears to be a severe underestimation of the FC term in the DFT calculation. This may be related to the DFT delocalization error, since SO coupling is not a major impact for the mercury-containing systems. A more in-depth comparison of DFT versus correlated wave function calculations would be needed in order to confirm this hypothesis. The RASSI performance is likewise not good and may indicate the lack of dynamic correlation, leading to the FC term to be strongly underestimated. If we assume instead, as in the experimental work,[103] that all tensor components are positive, we obtain 634 MHz at the RAS[5/75] level, which agrees well with experiment.

Table 3 collects additional data for NpF_6, including a breakdown of the HFC tensors into the principal components parallel || and perpendicular ⊥ to the Np−F bonds and results obtained without SO coupling (SR). The Np HFC tensor is isotropic, and therefore, the tensor components are only shown in order to demonstrate that the active spaces used do not break the symmetry. The results for each of the fluorines are likewise equivalent. We highlight the improvements in the fluorine $a_\perp$, in particular, upon inclusion of more occupied orbitals in the active space. Previous Dirac scattered wave calculations performed by Case[104] are also listed; the agreement with our best SO-RASSI calculation is very close. Case already emphasized the all-important spin polarization effects. In the approach of ref 104, the spin polarization effects were estimated based on separate nonrelativistic spin-polarized calculations. Nonetheless, it delivered excellent results. Interestingly, the fluorine isotropic HFCCs with and without SO coupling are nearly identical at the RAS[16/65] level due to error cancellation: in the SR calculation $a_\perp$ is severely overestimated in magnitude while $a_\parallel$ is severely underestimated.

Figure 1 displays the spin magnetization m_z for NpF_6 for selected CAS and RAS calculations. See refs 97 and 106 for details. A linear combination of the doublet state components diagonalizing the Zeeman interaction for a magnetic field along z was generated, and the component with $\langle S_z \rangle > 0$ was chosen to generate data for the plots. At the scalar relativistic level (SR, meaning absence of SO coupling), m_z corresponds to the usual spin density and integrates to $2M_S$ (= ±1 for the doublet state components considered here, counting the excess of occupied α

DOI: 10.1021/ct500988h
J. Chem. Theory Comput. 2015, 11, 538−549

versus β spin orbitals). With or without SO coupling, m_z integrates to $2\langle S_z\rangle$. We focus on the fluorine HFC.

The formally unpaired 5*f* orbital of Np is of δ symmetry with respect to all Np−F axes and therefore nonbonding at the SR level. With the small active space, there is indeed no spin density at the ligands, and correspondingly, the calculation (Table 3) gives no FC contribution for fluorine, a perfectly anisotropic SD mechanism, and no PSO contribution. The SO interaction mixes α spin f_δ with β spin f_π, leading to the presence of the negative lobes in the isosurface plot for CAS(1,7)-SO in Figure 1. The chosen quantization axis for the angular momenta is along *z*, which is vertical in Figure 1. In the plane showing the contour line plot, the negative spin density at the corresponding pair of fluorines is evident. With a quantization axis along *x* or *y*, the corresponding plots of m_x and m_y yield an equivalent picture for the two other fluorine pairs. The SO interaction leads to a sizable isotropic component in the SD mechanism (Table 3) and creates a nonzero PSO contribution, also with a sizable isotropic component. However, due to the fact that m_z vanishes along the Np−F axes there is still no FC contribution with CAS(1,7). Consequently the calculation severely underestimates the magnitude of the fluorine HFC in comparison with experiment and with the spin-polarized DFT results of Table 2.

The situation changes drastically when the active space is extended to allow for spin polarization. Table 3 shows that a sizable FC contribution arises at the SR level. The spin density is visible already as lobes in the isosurface plot. The contour line plots—in which the contour values go as low as 10^{-4} atomic units—clearly show the orbital interactions between Np and F that are created via the spin polarization afforded by the additional excitations. Spin polarization at the Np center creates a nonvanishing spin magnetization in the nodal planes of the SF CAS(1,7) spin density, which then further induces a sizable spin magnetization around the fluorine atoms and at the fluorine nuclei. The sign patterns appear somewhat different in the SO calculation, but as in the SF case, there is now a nonvanishing spin magnetization along the Np−F axes that allows for the FC mechanism to render $a_\parallel$ and $a_\perp$ to become more negative overall, compared to smaller active spaces, and agree better with experiment.

5. CONCLUSIONS AND OUTLOOK

The presented initial test calculations with a new module in the Molcas SO-RASSI program for electron−nucleus hyperfine coupling (HFC) tensors validate the implementation. SO coupling effects on HFC tensors in actinide systems can be very important both for the metal and for light ligands. In order to treat unpaired electrons in orbitals of low angular momentum at a heavy metal center, an extension to relativistic HFC operators will be implemented subsequently.

While the chosen approach with single excitations from most of the occupied orbitals included in the active space is not expected to be very accurate, it gives similar performance as hybrid DFT in the test calculations. However, there are several important advantages over KS-DFT with available approximate functionals that we will investigate in subsequent work. Chiefly among those is the ability to treat orbitally degenerate states where the single-reference nature of KS-DFT with currently available approximate functionals has difficulties. Examples of such situations were recently discussed by us in ref 97 in the context of EPR *g*-factor calculations for actinide complexes and in ref 106 in the context of calculating ligand NMR shifts. Another advantage with the SO-RASSI approach is that it is straightforward to determine the EPR parameters for low-energy excited states (e.g., from a 4*f* or 5*f* manifold) that may affect measurements made at ambient temperatures. Further, it may be possible to use the HFC approach within a multiconfigurational hybrid theory[107,108] that combines the advantages of wave function theory with the advantages of DFT.

AUTHOR INFORMATION

Corresponding Author

*E-mail: jochena@buffalo.edu.

Notes

The authors declare no competing financial interest.

ACKNOWLEDGMENTS

This research was supported by the U.S. Department of Energy, Office of Basic Energy Sciences, Heavy Element Chemistry program, under grant DE-FG02-09ER16066. We further acknowledge computer time and technical support by the Center for Computational Research (CCR) at the University at Buffalo. We thank Dr. B. Gao for assistance with creating the interface for the GEN1INT library.

REFERENCES

(1) Atherton, N. M. *Principles of Electron Spin Resonance*; Ellis Horwood Series in Physical Chemistry; Prentice Hall: New York, 1993; pp 38, 59−129.
(2) Eriksson, L. A. ESR hyperfine calculations. In *Encyclopedia of Computational Chemistry*; von Ragué Schleyer, P., Ed.; Wiley: Chichester, U.K., 1998; pp 952−958.
(3) Rieger, P. H. *Electron Spin Resonance. Analysis and Interpretation*; The Royal Society of Chemistry: Cambridge, U.K., 2007; pp 133−144.
(4) Harriman, J. E. *Theoretical Foundations of Electron Spin Resonance*; Academic Press: New York, 1978; pp 277−301.
(5) *Calculation of NMR and EPR Parameters. Theory and Applications*; Kaupp, M., Bühl, M., Malkin, V. G., Eds.; Wiley-VCH: Weinheim, 2004; pp 325−338.
(6) Pople, J. A.; Beveridge, D. L.; Dobosh, P. A. *J. Am. Chem. Soc.* **1968**, *90*, 4201−4209.
(7) Hameka, H. F.; Turner, A. G. *J. Magn. Reson.* **1985**, *64*, 66−75.
(8) Nakatsuji, H.; Kato, H.; Yonezawa, T. *J. Chem. Phys.* **1969**, *51*, 3175−3180.
(9) Chipman, D. M. *J. Chem. Phys.* **1979**, *71*, 761−768.
(10) Chipman, D. M. *Theor. Chem. Acc.* **1992**, *82*, 93−115.
(11) Sekino, H.; Bartlett, R. J. *J. Chem. Phys.* **1985**, *82*, 4225−4229.
(12) Kristiansen, P.; Veseth, L. *J. Chem. Phys.* **1986**, *84*, 2711−2719.
(13) Kristiansen, P.; Veseth, L. *J. Chem. Phys.* **1986**, *84*, 6336−6343.
(14) Kaupp, M.; Arbuznikov, A. V.; Heßelmann, A.; A, G. *J. Chem. Phys.* **2010**, *132*, 184107−10.
(15) Gauld, J. W.; Eriksson, L. A.; Radom, L. *J. Phys. Chem. A* **1997**, *101*, 1352−1359.
(16) Kossmann, S.; Neese, F. *J. Phys. Chem. A* **2010**, *114*, 11768−11781.
(17) Perera, S. A.; Watts, J. D.; Bartlett, R. J. *J. Chem. Phys.* **1994**, *100*, 1425−1434.
(18) Chang, S. Y.; Davidson, E. R.; Vincow, G. *J. Chem. Phys.* **1970**, *52*, 5596−5606.
(19) Vincow, G. *J. Phys. Chem.* **1971**, *75*, 3400−3410.
(20) Konishi, H.; Morokuma, K. *J. Am. Chem. Soc.* **1972**, *94*, 5603−5612.
(21) Ellinger, Y.; Subra, R.; Berthier, G. *J. Am. Chem. Soc.* **1978**, *100*, 4961−4963.
(22) Feller, D.; Davidson, E. R. *J. Chem. Phys.* **1984**, *80*, 1006−1017.
(23) Engels, B. *Theor. Chem. Acc.* **1993**, *86*, 429−437.
(24) Hohenberg, P.; Kohn, W. *Phys. Rev. B* **1964**, *136*, 864−871.

DOI: 10.1021/ct500988h
J. Chem. Theory Comput. 2015, 11, 538−549

(25) Kohn, W.; Sham, L. *Phys. Rev. A* **1965**, *140*, 1133−1138.
(26) Eriksson, L. A.; Malkin, V. G.; Malkina, O. L.; Salahub, D. R. *J. Chem. Phys.* **1993**, *99*, 9756−9763.
(27) Eriksson, L. A.; Malkina, O. L.; Malkin, V. G.; Salahub, D. R. *J. Chem. Phys.* **1994**, *100*, 5066−5075.
(28) Eriksson, L. A.; Malkin, V. G.; Malkina, O. L.; Salahub, D. R. *Int. J. Quantum Chem.* **1994**, *52*, 879−901.
(29) Ishii, N.; Shimizu, T. *Chem. Phys. Lett.* **1994**, *225*, 462−466.
(30) Neese, F. *J. Chem. Phys.* **2003**, *118*, 3939−3948.
(31) Kossmann, S.; Kirchner, B.; Neese, F. *Mol. Phys.* **2007**, *105*, 2049−2071.
(32) Pritchard, B.; Autschbach, J. *Inorg. Chem.* **2012**, *51*, 8340−8351.
(33) Verma, P.; Autschbach, J. *J. Chem. Theory Comput.* **2013**, *9*, 1052−1067.
(34) Bauschlicher, C. W., Jr.; Langhoff, S. R.; Partridge, H.; Chong, D. P. *J. Chem. Phys.* **1988**, *89*, 2985−2992.
(35) Engels, B.; Peyerimhoff, S. D. *Z. Phys. D* **1989**, *13*, 335−343.
(36) Engels, B.; Peyerimhoff, S. D.; Davidson, E. R. *Mol. Phys.* **1987**, *62*, 109−127.
(37) Feller, D.; Davidson, E. R. *J. Chem. Phys.* **1988**, *88*, 7580−7587.
(38) Bauschlicher, C. W., Jr. *J. Chem. Phys.* **1990**, *92*, 518−521.
(39) Engels, B. *Chem. Phys. Lett.* **1991**, *179*, 398−404.
(40) Engels, B. *J. Chem. Phys.* **1994**, *100*, 1380−1386.
(41) Suter, H.; Engels, B. *J. Chem. Phys.* **1994**, *100*, 2936−2942.
(42) Suter, H.; Huang, M.−B.; Engels, B. *J. Chem. Phys.* **1994**, *101*, 7686−7691.
(43) Perić, M.; Engels, B. *J. Mol. Spectrosc.* **1995**, *174*, 334−352.
(44) Fernandez, B.; Jørgensen, P.; Byberg, J.; Olsen, J.; Helgaker, T.; Jensen, H. J. A. *J. Chem. Phys.* **1992**, *97*, 3412−3419.
(45) Yanai, T.; Kurashige, Y.; Mizukami, W.; Chalupský, J.; Lan, T. N.; Saitow, M. *Int. J. Quantum Chem.* **2014**, DOI: 10.1002/qua.24808.
(46) Lan, T. N.; Kurashige, Y.; Yanai, T. *J. Chem. Theory Comput.* **2014**, DOI: 10.1021/ct5007778.
(47) Engels, B. Ab initio post-Hartree−Fock calculations of hyperfine coupling tensors and their comparison with DFT approaches. In *Calculation of NMR and EPR Parameters*; Kaupp, M., Bühl, M., Malkin, V. G., Eds.; Wiley-VCH: Weinheim, 2004.
(48) Munzarová, M.; Kaupp, M. *J. Phys. Chem. A* **1999**, *103*, 9966−9983.
(49) Pyykkö, P. *Chem. Rev.* **1988**, *88*, 563−594.
(50) Autschbach, J. *J. Chem. Phys.* **2012**, *136*, 150902.
(51) Malkin, I.; Malkina, O. L.; Malkin, V. G.; Kaupp, M. *Chem. Phys. Lett.* **2004**, *396*, 268−276.
(52) Malkin, E.; Malkin, I.; Malkina, O. L.; Malkin, V. G.; Kaupp, M. *Phys. Chem. Chem. Phys.* **2006**, *8*, 4079−4085.
(53) Sandhoefer, B.; Kossmann, S.; Neese, F. *J. Chem. Phys.* **2013**, *138*, 104102.
(54) Aquino, F.; Pritchard, B.; Autschbach, J. *J. Chem. Theory Comput.* **2012**, *8*, 598−609.
(55) Verma, P.; Autschbach, J. *J. Chem. Theory Comput.* **2013**, *9*, 1932−1948.
(56) Filatov, M.; Cremer, D. *J. Chem. Phys.* **2004**, *121*, 5618−5622.
(57) Filatov, M.; Zou, W.; Cremer, D. *J. Phys. Chem. A* **2012**, *116*, 3481−3486.
(58) Filatov, M.; Cremer, D. *J. Chem. Phys.* **2005**, *123*, 124101.
(59) van Lenthe, E.; van der Avoird, A.; Wormer, P. E. S. *J. Chem. Phys.* **1998**, *108*, 4783−4796.
(60) Autschbach, J.; Patchkovskii, S.; Pritchard, B. *J. Chem. Theory Comput.* **2011**, *7*, 2175−2188.
(61) Quiney, H. M.; Belanzoni, P. *Chem. Phys. Lett.* **2002**, *353*, 253−258.
(62) Malkin, E.; Repisky, M.; Komorovsky, S.; Mach, P.; Malkina, O. L.; Malkin, V. G. *J. Chem. Phys.* **2011**, *134*, 044111.
(63) Arbuznikov, A. V.; Vaara, J.; Kaupp, M. *J. Chem. Phys.* **2004**, *120*, 2127−2139.
(64) Patchkovskii, S.; Schreckenbach, G. Calculation of EPR g-tensors with density functional theory. In *Calculation of NMR and EPR Parameters. Theory and Applications*; Kaupp, M., Bühl, M., Malkin, V. G., Eds.; Wiley-VCH: Weinheim, 2004; pp 505−532.
(65) Tatchen, J.; Kleinschmidt, M.; Marian. *J. Chem. Phys.* **2009**, *130*, 154106.
(66) Ganyushin, D.; Neese, F. *J. Chem. Phys.* **2013**, *138*, 104113.
(67) Vad, M. S.; N, P. M.; Nørager, A.; Jensen, H. J. A. *J. Chem. Phys.* **2013**, *138*, 214106.
(68) Bolvin, H. *ChemPhysChem* **2006**, *7*, 1575−1589.
(69) Vancoillie, S.; Malmqvist, P.-Å.; Pierloot, K. *ChemPhysChem* **2007**, *8*, 1803−1815.
(70) Malmqvist, P.-Å.; Ross, B. O. *Chem. Phys. Lett.* **1989**, *155*, 189−194.
(71) Malmqvist, P.-Å.; Ross, B. O.; Schimmelpfennig, B. *Chem. Phys. Lett.* **2002**, *357*, 230−240.
(72) Aquilante, F.; Vico, L. D.; Ferré, N.; Ghigo, G.; Malmqvist, P.-Å.; Neogrády, P.; Pedersen, T. B.; Pitoňák, M.; Reiher, M.; Roos, B. O.; Serrano−Andrés, L.; Urban, M.; Veryazov, V.; Lindh, R. *J. Comput. Chem.* **2010**, *31*, 224.
(73) Aquino, F.; Govind, N.; Autschbach, J. *J. Chem. Theory Comput.* **2011**, *7*, 3278−3292.
(74) Autschbach, J.; Ziegler, T. *Coord. Chem. Rev.* **2003**, *238/239*, 83−126.
(75) Pritchard, B. *Calculation of magnetic properties of paramagnetic molecules*. Ph.D. Thesis, University at Buffalo, State University of New York, 2014.
(76) Gao, B.; Thorvaldsen, A. J.; Ruud, K. *Int. J. Quantum Chem.* **2011**, *111*, 858.
(77) Gerloch, M.; McMeeking, R. F. *J. Chem. Soc., Dalton Trans.* **1975**, 2443−2451.
(78) Hess, B. A.; Marian, C. M.; Wahlgren, U.; Gropen, O. *Chem. Phys. Lett.* **1996**, *251*, 365.
(79) Christiansen, O.; Gauss, J.; Schimmelpfennig, B. *Phys. Chem. Chem. Phys.* **2000**, *2*, 965−971.
(80) Vahtras, O.; Engström, M.; Schimmelpfennig, B. *Chem. Phys. Lett.* **2002**, *351*, 424−430.
(81) Schwarz, W. H. E.; van Wezenbeek, E. M.; Baerends, E. J.; Snijders, J. G. *J. Phys. B: At., Mol. Opt. Phys.* **1989**, *22*, 1515−1530.
(82) Douglas, M.; Kroll, N. M. *Ann. Phys.* **1974**, *82*, 89−115.
(83) Hess, B. A. *Phys. Rev. A* **1986**, *33*, 3742−3748.
(84) Valiev, M.; Bylaska, E. J.; Govind, N.; Kowalski, K.; Straatsma, T. P.; van Dam, H. J. J.; Wang, D.; Nieplocha, J.; Apra, E.; Windus, T. L.; de Jong, W. A. *Comput. Phys. Commun.* **2010**, *181*, 1477−1489.
(85) Van Wüllen, C. *J. Chem. Phys.* **2009**, *130*, 194109.
(86) Adamo, C.; Barone, V. *J. Chem. Phys.* **1999**, *110*, 6158−6170.
(87) Amsterdam Density Functional (ADF) program suite. http://www.scm.com/ (accessed 02/2014).
(88) Becke, A. D. *Phys. Rev. A* **1988**, *38*, 3098−3100.
(89) Perdew, J. P. *Phys. Rev. B* **1986**, *33*, 8822−8824.
(90) Notter, F.-P.; Bolvin, H. *J. Chem. Phys.* **2009**, *130*, 184310.
(91) Neese, F.; Solomon, E. I. Interpretation and Calculation of Spin-Hamiltonian Parameters in Transition Metal Complexes. In *Magnetism: Molecules to Materials IV*; Miller, J. S., Drillon, M., Eds.; Wiley-VCH: 2002 page 400.
(92) Arratia−Pérez, R.; Hernandez−Acevedo, L.; Malli, G. L. *J. Chem. Phys.* **2004**, *121*, 7743−7747.
(93) Butler, J. E.; Hutchison, C. A., Jr *J. Chem. Phys.* **1981**, *74*, 3102−3119.
(94) Roos, B. O.; Lindh, R.; Malmqvist, P.-A.; Veryazov, V.; Widmark, P.-O. *J. Phys. Chem. A* **2004**, *108*, 2851.
(95) Roos, B. O.; Lindh, R.; Malmqvist, P.-Å.; Veryazov, V.; Widmark, P.-O. *Chem. Phys. Lett.* **2005**, *409*, 295−299.
(96) Roos, B. O.; Lindh, R.; Malmqvist, P.-Å.; Veryazov, V.; Widmark, P.-O. *J. Phys. Chem. A* **2005**, *109*, 6575.
(97) Gendron, F.; Páez-Hernández, D.; Notter, F.-P.; Pritchard, B.; Bolvin, H.; Autschbach, J. *Chem.—Eur. J.* **2014**, *20*, 7994−8011.
(98) Weltner, W. Jr. *Magnetic Atoms and Molecules*; Dover Publications, Inc.: New York, 1983.
(99) Holmberg, R. W. *J. Chem. Phys.* **1969**, *51*, 3255−3260.
(100) Van Zee, R. J.; Ferrante, R. F.; Weltner, W., Jr. *J. Chem. Phys.* **1985**, *83*, 6181−6187.

DOI: 10.1021/ct500988h
J. Chem. Theory Comput. 2015, 11, 538−549

(101) De Vore, T. C.; Weltner, W. *J. Am. Chem. Soc.* **1977**, *99*, 4700−4703.
(102) Knight, L. B., Jr.; Weltner, W., Jr. *J. Chem. Phys.* **1971**, *55*, 2061−2070.
(103) Knight, L. B., Jr.; Fisher, T. A.; Wise, M. B. *J. Chem. Phys.* **1981**, *74*, 6009−6013.
(104) Case, D. A. *J. Chem. Phys.* **1985**, *83*, 5792−5796.
(105) Autschbach, J.; Pritchard, B. *Theor. Chem. Acc.* **2011**, *129*, 453−466.
(106) Gendron, F.; Pritchard, B.; Bolvin, H.; Autschbach, J. *Inorg. Chem.* **2014**, *53*, 8577−8592.
(107) Fromager, E.; Toulouse, J.; Jensen, H. J. A. *J. Chem. Phys.* **2007**, *126*, 074111.
(108) Sharkas, K.; Toulouse, J.; Savin, A.; Jensen, H. J. A. *J. Chem. Phys.* **2012**, *137*, 044104−10.

DOI: 10.1021/ct500988h
J. Chem. Theory Comput. 2015, 11, 538−549